LA-9168-MS

C.3

Average Neutronic Properties of "Prompt" Fission Products

Los Alamos
Los Alamos National Laboratory
Los Alamos, New Mexico 87545

DISCLAIMER

Average Neutronic Properties of

"Prompt" Fission Products

D. G. Foster, Jr.
E. D. Arthur

AVERAGE NEUTRONIC PROPERTIES OF "PROMPT" FISSION PRODUCTS

by

D. G. Foster, Jr., and E. D. Arthur

ABSTRACT

We describe here calculations of the average neutronic properties of the ensemble of fission products produced by fast-neutron fission of ^{235}U and ^{239}Pu, where the properties are determined before the first beta decay of any of the fragments. For each case we approximate the ensemble by a weighted average over 10 selected nuclides, whose properties we calculate using nuclear-model parameters deduced from the systematic properties of other isotopes of the same elements as the fission fragments. The calculations were performed primarily with the COMNUC and GNASH statistical-model codes. The results, available in ENDF/B format, include cross sections, angular distributions of neutrons, and spectra of neutrons and photons, for incident-neutron energies between 10^{-5} eV and 20 MeV. Over most of this energy range, we find that the capture cross section of ^{239}Pu fission fragments is systematically a factor of two to five greater than for ^{235}U fission fragments.

I. INTRODUCTION AND SUMMARY

Neutronic calculations performed on a system undergoing a rapid chain reaction require cross sections and related data for the resulting fission fragments before they have had time to undergo beta decay. In general, the yields of the fragments are reasonably well known, but they are too short-lived for direct measurements of their neutronic properties to be feasible. Therefore, we must resort to calculations using nuclear-model codes with input data deduced from the systematic properties of isotopes that lie much closer to the line of beta stability than the fragments. Since there are approximately 1000 nuclides involved, we must content ourselves with a suitable average over a small but representative sample of the nuclides.

This report describes such calculations for the fragments from fast-neutron-induced fission of ^{235}U and ^{239}Pu. As noted in preliminary reports,[1-3] we have approximated the ensemble of fragments by taking a yield-weighted average

1

over 10 nuclides for each fissile species, selected from the peaks and half-height points of the low-mass and high-mass parts of the yield curve, using pairs having even and odd mass. There is enough difference between ^{235}U and ^{239}Pu that ^{138}Xe is the only target nuclide common to both sets, so we must consider 19 nuclides altogether. These are shown in Fig. 1. For incident-neutron energies up to 20 MeV, we must include the (n,γ), elastic-scattering, inelastic-scattering, (n,2n), and (n,3n) reactions on each of these targets, which enlarges the data set to include 44 residual nuclides.

All of our calculations used spherical optical models and a Hauser-Feshbach statistical treatment of compound nuclei, modified to include pre-equilibrium effects in the compound state formed by the target and the incoming neutron. These models were embodied primarily in three computer programs: COMNUC,[4] GNASH,[5] and SCAT.[6]

The principal results of this work are summarized in Figs. 2 - 10, which exhibit the integrated neutron and photon-production cross sections for each reaction, a simple treatment of cross sections below 1 keV, a comparison of the capture cross sections for the two cases, the energy-dependent Legendre coefficients for elastic scattering, and an example of a coupled energy-angular distribution of secondary neutrons. As described in detail below, we have used the Kalbach-Mann formalism[7] to approximate all secondary-neutron angular distributions except those for elastic scattering and inelastic scattering to discrete states in the target-nuclides. Figure 11 illustrates a modified form of these distributions, which are independent of target nuclide, reaction, and incident-neutron energy.

The motivation for these calculations was to provide cross-section sets for applied calculations. In this context, the most noteworthy difference between the two fissionable nuclides is in the capture cross section of the fission fragments, which is about a factor of five greater for ^{239}Pu than for ^{235}U for incident neutrons below 1 eV, and about a factor of two greater above 1 keV (except near 4 MeV). We believe that this difference is real and results directly from the small systematic difference between the two fragment-mass distributions relative to nearby closed shells.

II. INPUT DATA

It is obvious that the preparation of credible sets of input data is the most difficult part of this program. Techniques for estimating consistent nuclear parameters far from the line of beta stability have been evolving steadily

2
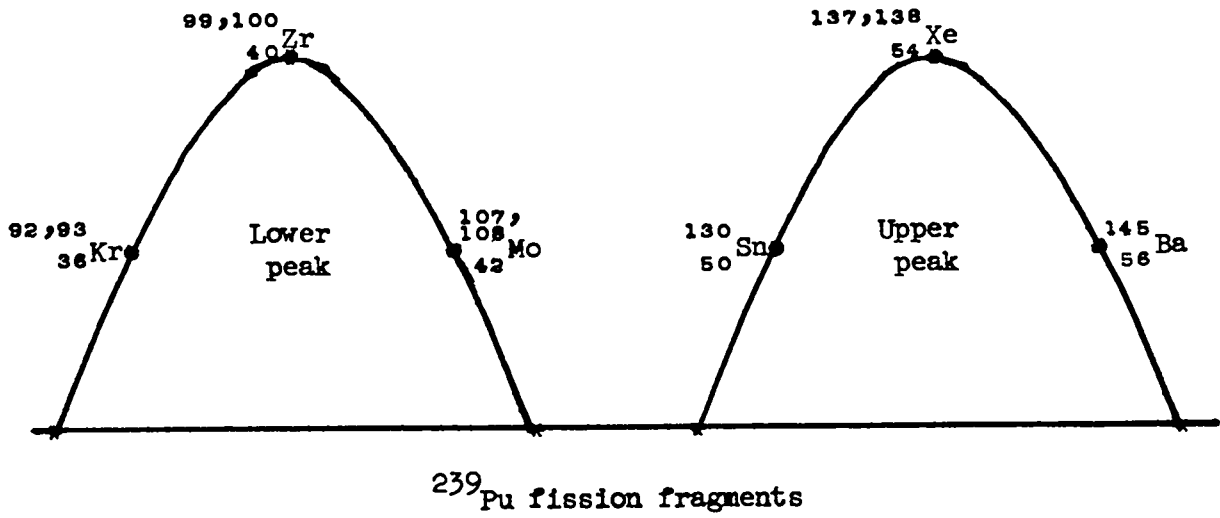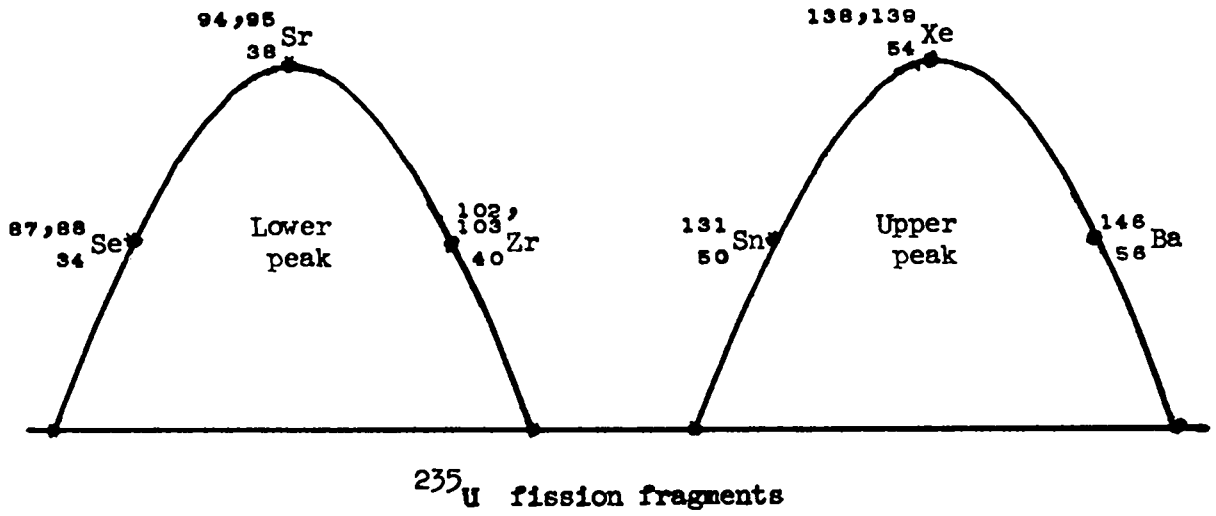
Figure 1. Target nuclides used in this work.

Figure 2.   Neutron cross sections of prompt fragments from
            fast fission of ^{235}U.
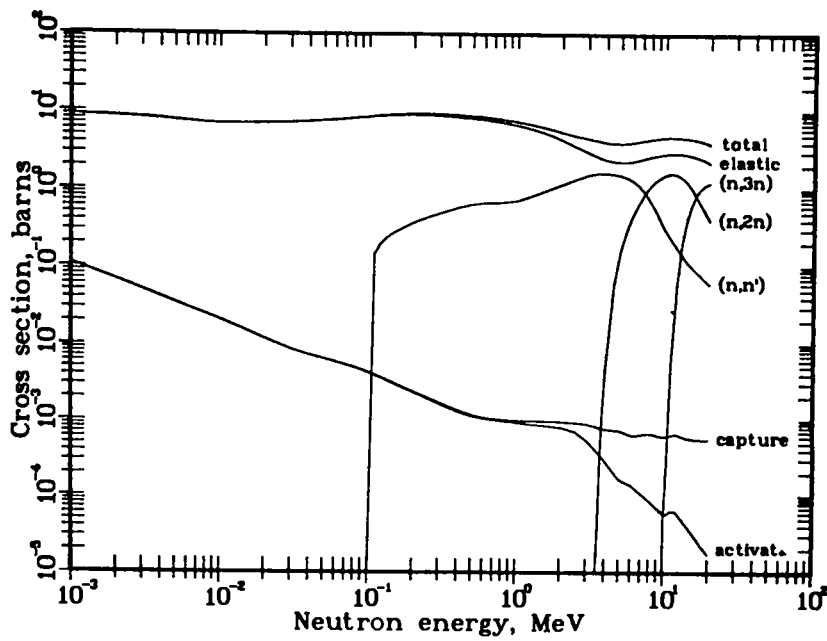
Figure 3.   Neutron cross sections of prompt fragments from fast
            fission of ^{239}Pu.
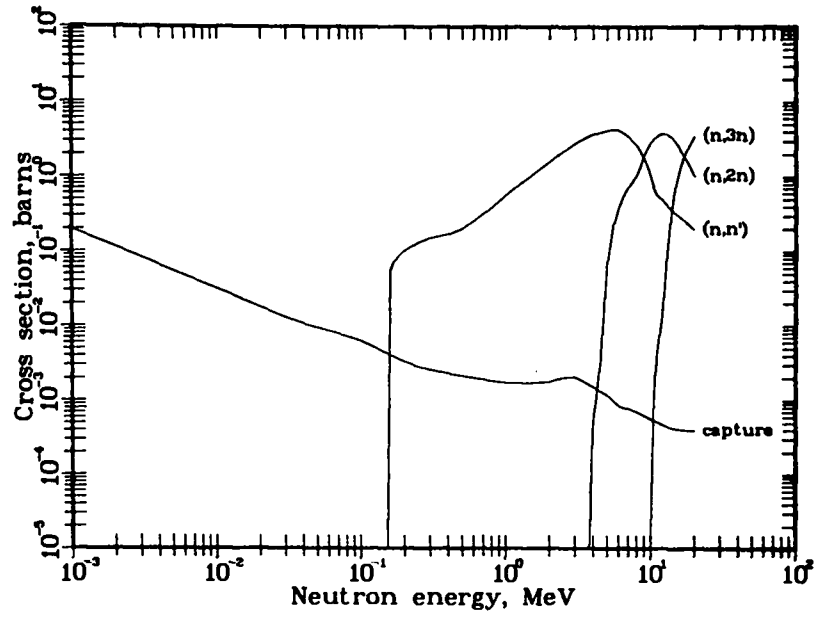
Figure 4. Photon-production cross sections of prompt fragments from fast fission of ^{235}U.
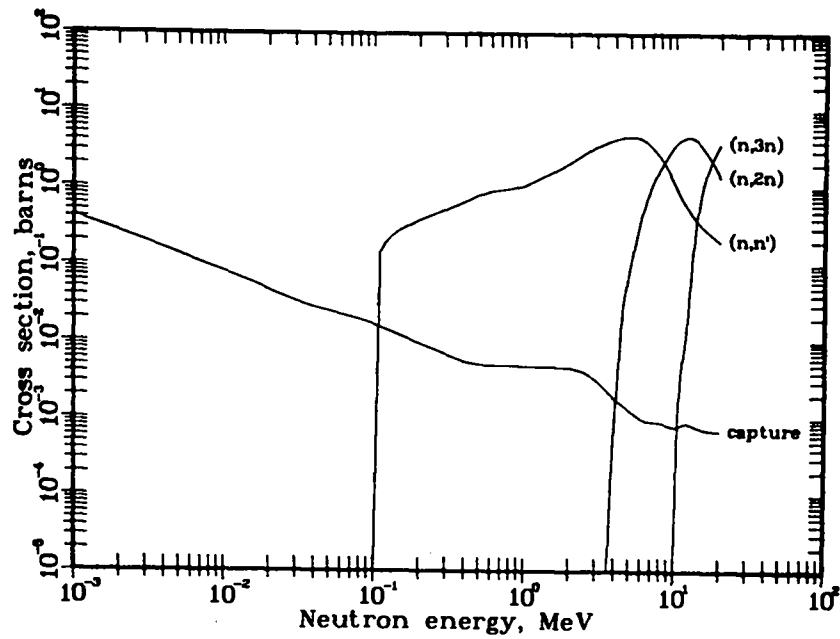
Figure 5. Photon-production cross sections of prompt fragments from fast fission of ^{239}Pu.
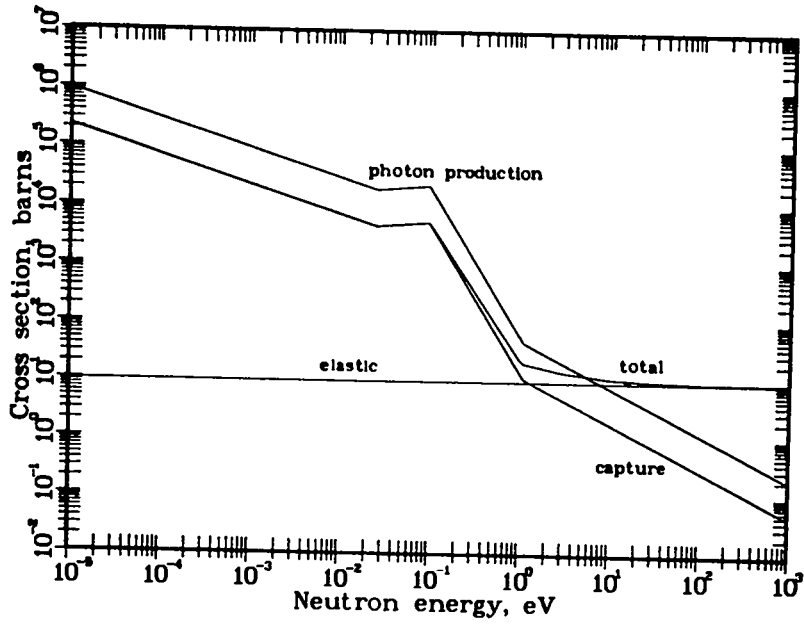
Figure 6. Slow-neutron cross sections of ^{235}U fission fragments.
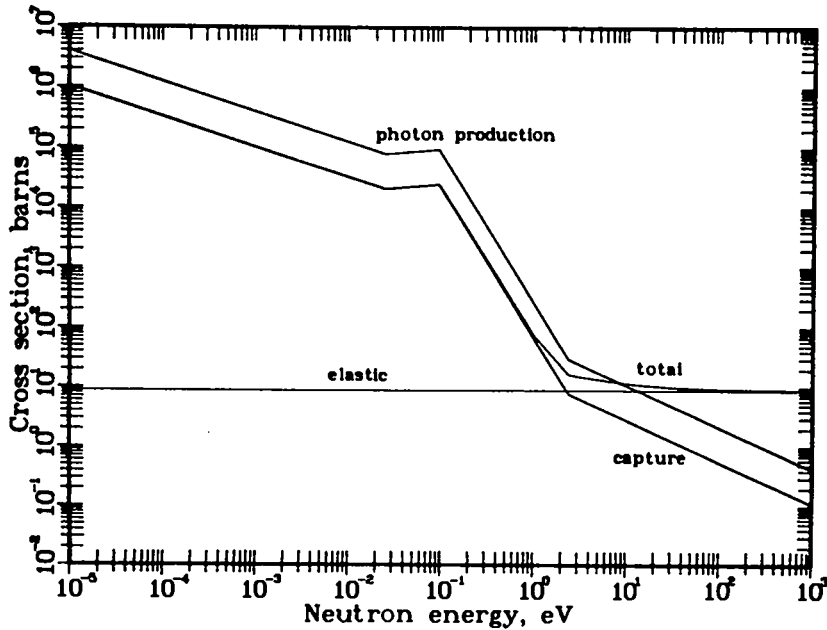
Figure 7. Slow-neutron cross sections of ^{239}Pu fission fragments.
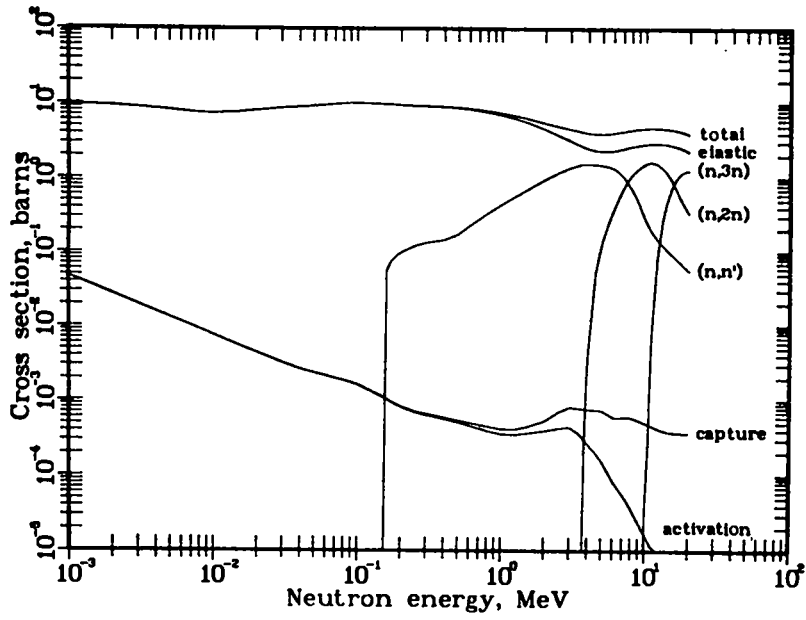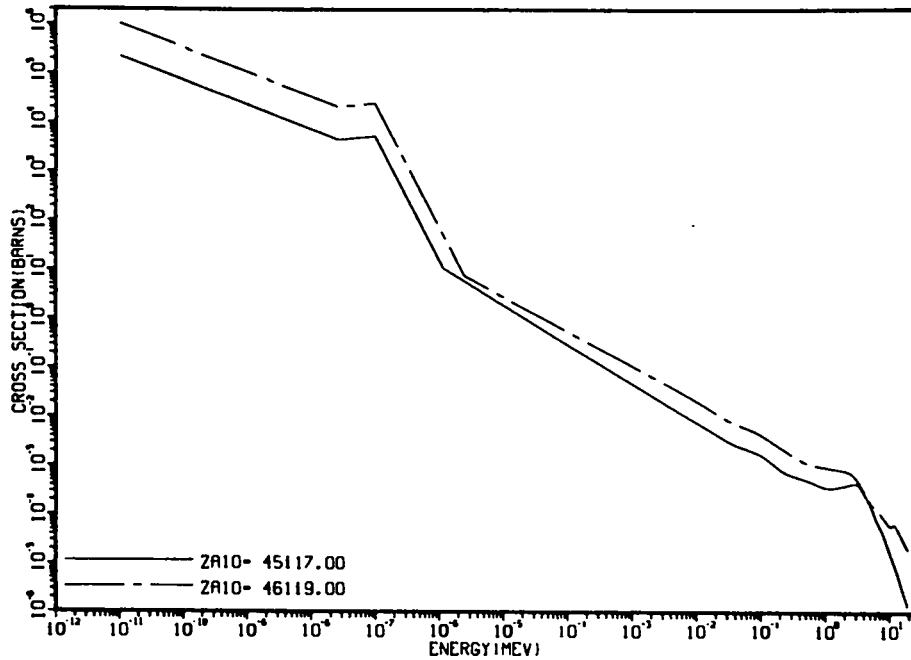
Figure 8.   Comparison of the calculated capture cross sections of prompt
fragments from fast fission of ^{235}U (solid line) and ^{239}Pu
(broken line). The ZAID identifier for each case is that used
in the ENDF/B version of this work and represents the average
atomic and mass numbers of the respective fragments, rounded
to the nearest integer.

Figure 9.   Legendre coefficients of elastic scattering from ^{235}U fission
fragments. The coefficients for ^{239}Pu are almost identical to
these. Note that for the first four partial waves the even
coefficient dominates at low energy, whereas at higher energy
the odd coefficient is the greater for all partial waves.

7

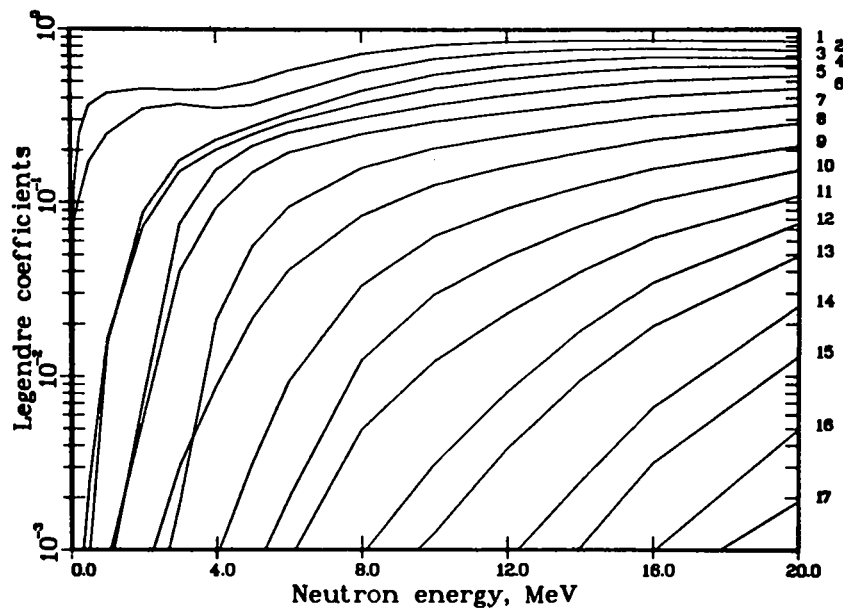| MEV | SPECTRUM | PREEQ. FRACT. | \- \- \- \- \- \- \- \- \- \- LEGENDRE COEFFICIENTS \- \- \- \- \- \- \- \- \- \- | | | | | | | |
			1	2	3	4	5	6	7	8
0.00	1.539E-03	.080	.0015	.0021						
0.05	1.562E-03	.080	.0015	.0021						
0.10	1.585E-03	.080	.0015	.0021						
0.15	1.609E-03	.080	.0015	.0021						
0.20	1.635E-03	.080	.0015	.0021						
0.25	1.661E-03	.080	.0015	.0021						
0.30	1.702E-03	.080	.0015	.0021						
0.40	1.760E-03	.080	.0015	.0021						
0.50	1.822E-03	.080	.0015	.0021						
0.60	1.923E-03	.094	.0018	.0029						
0.80	2.069E-03	.133	.0029	.0055	.0001	.0001				
1.00	2.252E-03	.133	.0029	.0055	.0001	.0001				
1.25	2.335E-03	.169	.0041	.0082	.0002	.0001				
1.50	2.868E-03	.169	.0041	.0082	.0002	.0001				
1.75	3.614E-03	.226	.0061	.0109	.0004	.0002				
2.0	5.914E-03	.268	.0078	.0125	.0006	.0002				
2.5	1.002E-02	.340	.0110	.0152	.0009	.0002				
3.0	1.794E-02	.415	.0151	.0180	.0013	.0003				
3.5	3.170E-02	.501	.0203	.0207	.0018	.0003				
4.0	4.265E-02	.593	.0265	.0233	.0024	.0004				
4.5	6.453E-02	.594	.0295	.0262	.0027	.0004				
5.0	1.297E-01	.637	.0355	.0290	.0032	.0005				
5.5	1.945E-01	.719	.0439	.0315	.0039	.0005				
6.0	2.050E-01	.769	.0517	.0342	.0045	.0005				
6.5	2.009E-01	.809	.0600	.0370	.0051	.0006				
7.0	1.987E-01	.852	.0694	.0397	.0058	.0006				
7.5	1.912E-01	.900	.0805	.0424	.0066	.0007				
8.0	1.785E-01	.931	.0909	.0451	.0072	.0007				
8.5	1.488E-01	.950	.1010	.0478	.0078	.0007				
9.0	1.180E-01	.969	.1021	.0484	.0077	.0006	.000	-.0001		
9.5	9.143E-02	.988	.1030	.0501	.0075	.0009	.000	.0002	.000	.0002
10.0	6.979E-02	.984	.0922	.0500	.0066	.0006	.000	-.0003	.000	.0002
10.5	4.983E-02	.981	.0760	.0419	.0052	-.0005	.000	-.0006	.000	-.0002
11.0	3.240E-02	.932	.0404	.0274	.0027	-.0006	.000	-.0008	.000	-.0004
11.644										
		AVERAGE:	.0669	.0382	.0054	.0005				

Figure 10. Energy-angular distribution for inelastic scattering from ^{235}U fission fragments at 12 MeV. The spectrum is normalized to unit integral. Note that the spectrum-weighted average angular distribution suppresses the higher Legendre moments.
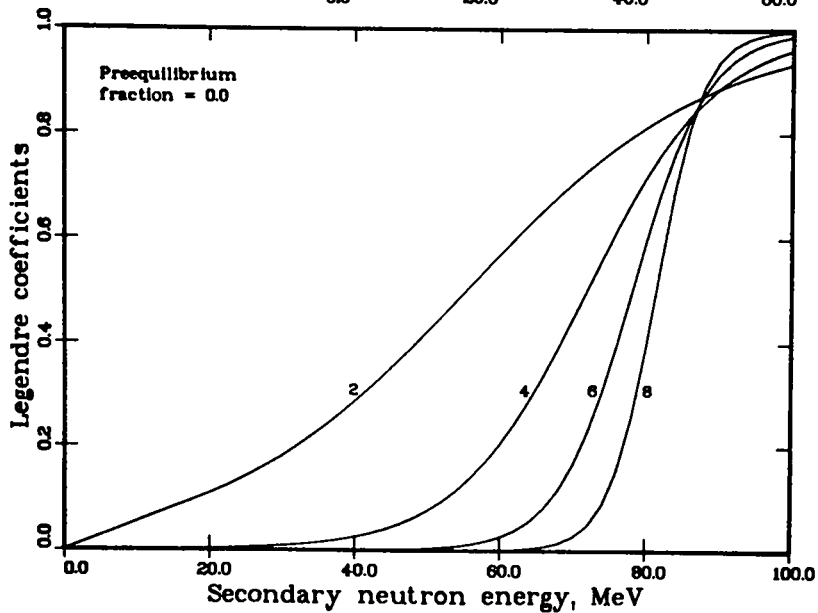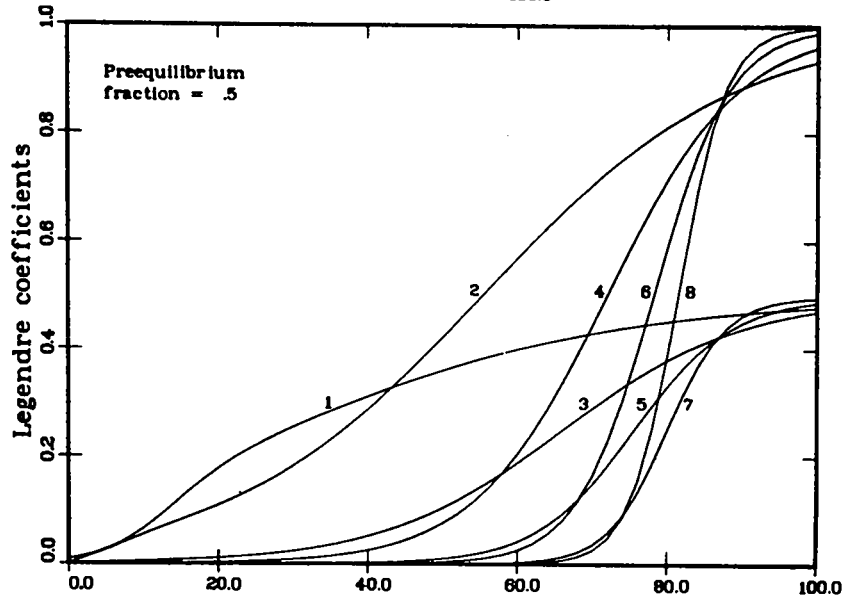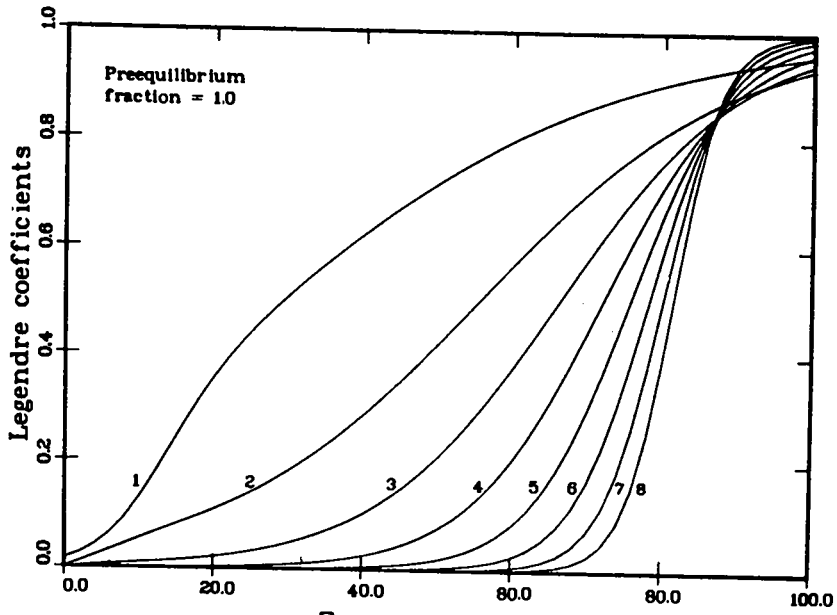
Figure 11. Modified Kalbach-Mann Legendre coefficients for three pre-equilibrium fractions.

for a number of years. Wherever experimental tests have been possible, for example in the recent work[8] on mass-90 nuclides, the results have been encouraging. We derive parameters to go into the nuclear models by fitting observations made on several stable isotopes of the element in question. Each fit yields a linear function of $\eta \equiv (N-Z)/A$, which supplies a crude extrapolation into the neutron-rich region of the primary fission fragments. We are confident that our results are an improvement over earlier estimates of the average properties of fission fragments. Nevertheless, wherever extrapolation produces a large change in a parameter, the uncertainty in its value is necessarily of the same order of magnitude as its value.

A. Target Nuclides

Our results are based on weighted averages over specific nuclides chosen from the peaks and half-height points of the appropriate fission-fragment yield curves. Only the half-height points for the heavy-fragment peak lie close to integral values of A. Accordingly, for the remaining points we have used even-odd pairs of isotopes of the same element, whose masses bracket the desired values. These are shown in Fig. 1. Each average includes five odd- and five even-mass nuclides. Altogether, we have used 19 isotopes of 10 elements; only ^{138}Xe occurs in both averages.

B. Parameters for the Spherical Optical Model

It is vital that parameters for a spherical neutron optical model describe the interaction correctly over a wide range of incident-neutron energies because we are interested simultaneously in good compound-nucleus-formation cross sections for (n,xn) reactions and a reasonable description of the emission of low-energy neutrons. Following the technique of Delaroche, Lagrange, and Salvy,[9] we fit parameters using both total cross sections measured over a wide range of neutron energies and low-energy s- and p-wave strength functions. By such analyses of isotopic data we can extract a linear dependence on η for both real and imaginary parts of the potential, in addition to the usual linear dependence on incident energy. This must be done very carefully, however, because the required extrapolation to neutron-rich fragments is of the same order of magnitude as the quantities themselves. As an example, Fig. 12 illustrates our fit to total cross sections of xenon, while Fig. 13 compares the corresponding s-wave strength functions to experimental values for six different values of η. The optical parameters that result, along with those for the other nuclides involved in these calculations, are listed in Table I.*

*The parameters for molybdenum are from Ref. 10.

10
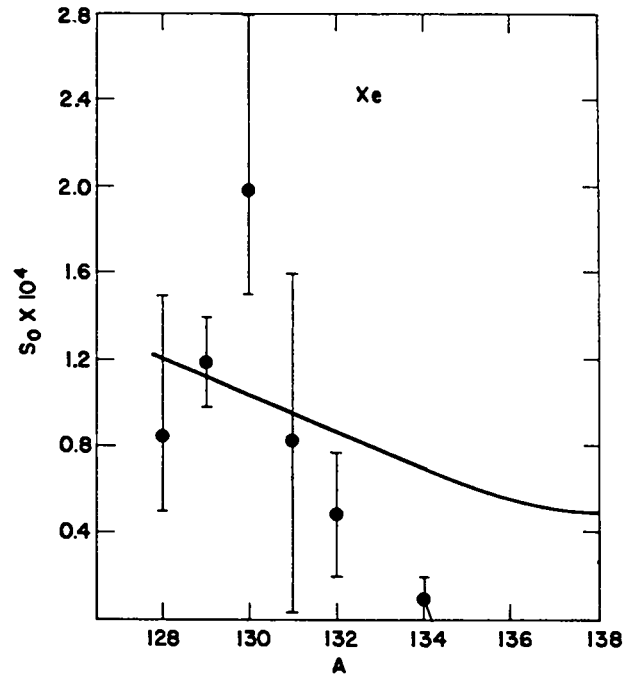
Figure 12. Comparison of calculated and experimental values for the xenon total cross section.
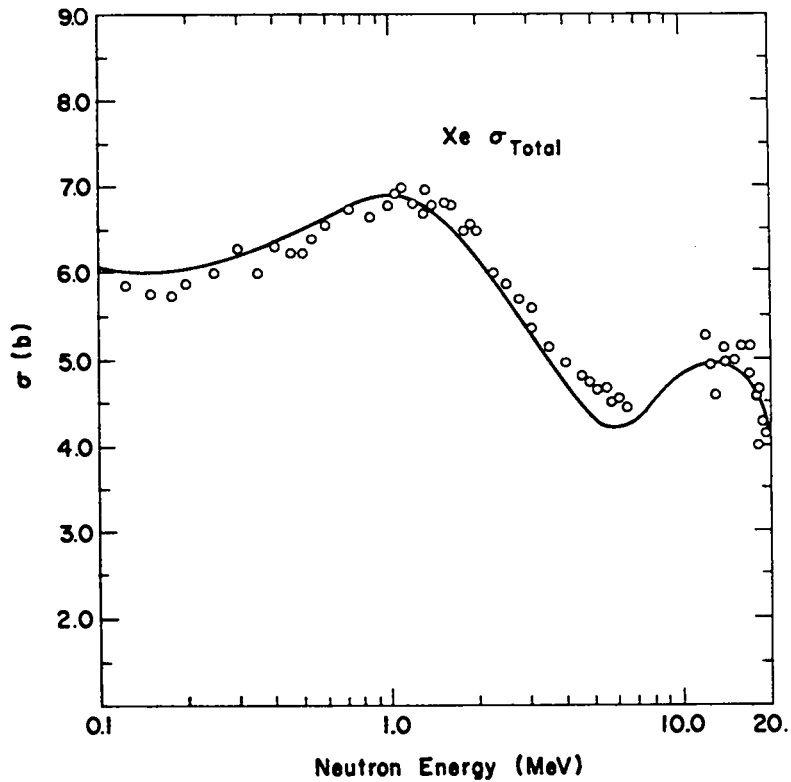
Figure 13. Calculated and experimental dependence of the s-wave strength function S_0 for isotopes of xenon.

TABLE I

SPHERICAL OPTICAL PARAMETERS[a]

Element	V_0	V_1	α	r_r	a_r	W_0	W_1	β	r_i	a_i	W'_0
Se	54.8	43	−0.35	1.24	0.62	12.5	33	0.36	1.26	0.65	14.5
Kr	52.75	22	−0.34	1.24	0.62	10.1	35	0.5	1.26	0.65	13.5
Sr	49.4	0	−0.15	1.24	0.62	8.5	36	0.5	1.26	0.58	12.9
Zr	48.6	0	−0.33	1.24	0.62	7.9	35	0.3	1.26	0.58	11.
Mo	50.8	17	−0.22	1.24	0.62	4.8	7	0.45	1.26	0.58	9.75[b]
Sn	56.3	50	−0.28	1.25	0.57	4.4	15	0.5	1.25	0.56	9.5
Xe	55.4	50	−0.35	1.25	0.65	12.8	50	0.4	1.25	0.56	17.1
Ba	49.0	22	−0.15	1.25	0.74	7.8	32	0.48	1.25	0.58	13

[a]Real and imaginary (Saxon derivative) forms used were

$V = V_0 - V_1 \eta + \alpha E$

$W = W_0 - W_1 \eta + \beta E$

$W_{max} = W'_0 - W_1 \eta$, with V and W in MeV; r_r, a_r, r_i and a_i in fm.

Spin-orbit values used were

$V_{SO} = 6.2$ MeV, $r_{SO} = 1.12$ fm, $a_{SO} = 0.47$ fm for Se, Kr, Sr, Zr, and Mo isotopes.

$V_{SO} = 7.5$ MeV, $r_{SO} = 1.25$ fm, $a_{SO} = 0.65$ fm for Sn, Xe, and Ba isotopes.

[b]These parameters are from Ref. 10.

The values for V_1 and W_1 shown in Table I are usually larger than those determined from fits to such data as elastic scattering from separated isotopes in the MeV region. The reason for this discrepancy is not clear, but it is consistent with similar analyses by Newstead and Delaroche.[11] Wherever possible, we also test our parameters against other types of measurements, as illustrated by the (n,2n) cross sections of ^{90}Zr and ^{112}Sn shown in Fig. 14.

C. Photon Transmission Coefficients

For calculating capture cross sections and describing competition between photon and particle emission, we base our photon-transmission coefficients on gamma-ray strength functions[8] instead of normalizing them to the customary ratio $\langle R \rangle \equiv 2\pi \langle \Gamma_\gamma \rangle / \langle D \rangle$, in which the average gamma-ray width $\langle \Gamma_\gamma \rangle$ and average level spacing $\langle D \rangle$ are determined independently. For unstable nuclei both $\langle \Gamma_\gamma \rangle$ and $\langle D \rangle$ can only be estimated from their average behavior over the mass range of interest, and both are subject to large fluctuations.

Instead, we define a gamma-ray strength function $f(\varepsilon_\gamma)$ of photon energy ε_γ such that

$$\frac{\langle R \rangle}{2\pi} = \int_0^{S_n} f(\varepsilon_\gamma) \, \varepsilon_\gamma^3 \, \rho(S_n - \varepsilon_\gamma) \, d\varepsilon_\gamma \quad , \tag{1}$$

in which S_n is the neutron separation energy and $\rho(E)$ is the level-density function in the compound system. If we assume that this strength function has a giant-dipole-resonance form given by

$$f_{E1}(\varepsilon\gamma) = \frac{k \, \varepsilon_\gamma \, \Gamma_{gdr}}{(\varepsilon_\gamma \Gamma_{gdr})^2 + (\varepsilon_\gamma^2 - E_{gdr}^2)^2} \quad , \tag{2}$$

then the constant k in Eq. (2) can be determined from fits to capture cross sections and spectra of stable isotopes. This strength function should not fluctuate so rapidly as $\langle R \rangle$; thus, one can extrapolate it into the neutron-rich region with greater confidence. The resulting equivalent values of $\langle R \rangle$ are given in Table II for each of the required nuclides in this program.

We can illustrate this behavior using the calculated gamma-ray strength functions for several isotopes of tin, which are shown in Fig. 15. Note that the extracted strength function varies from isotope to isotope by less than 50%. In contrast, the conventional $\langle R \rangle$ changes by a factor of 40 between ^{119}Sn and ^{120}Sn.
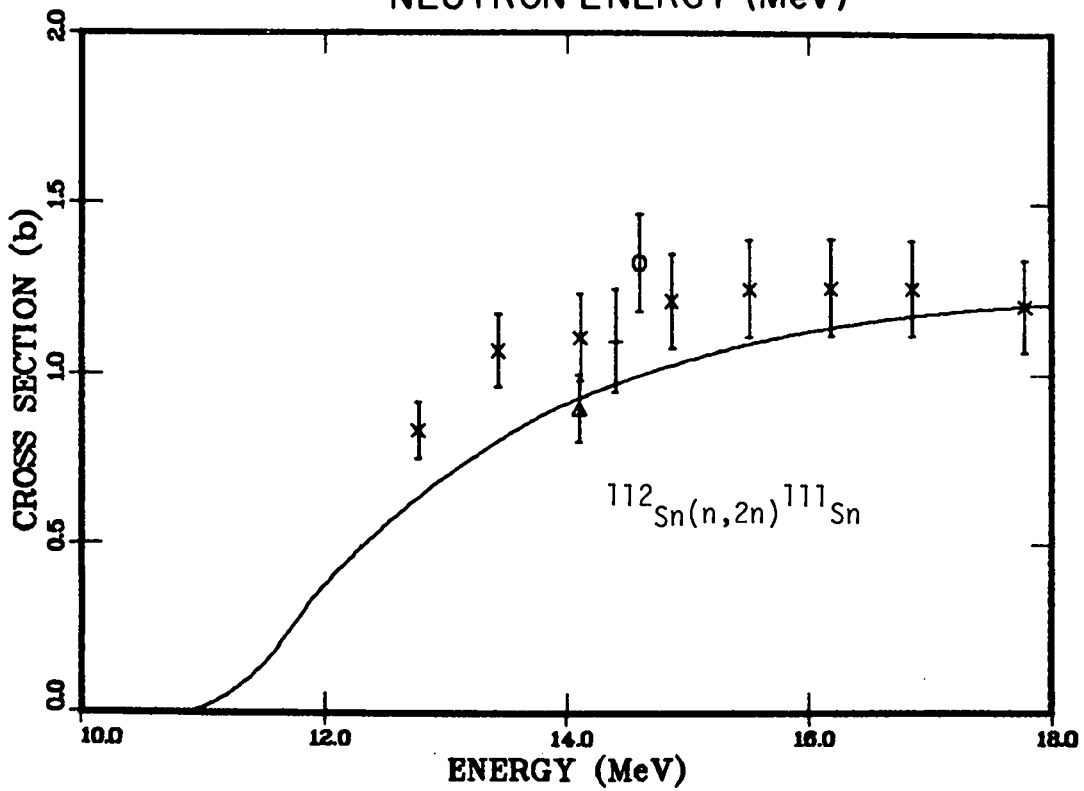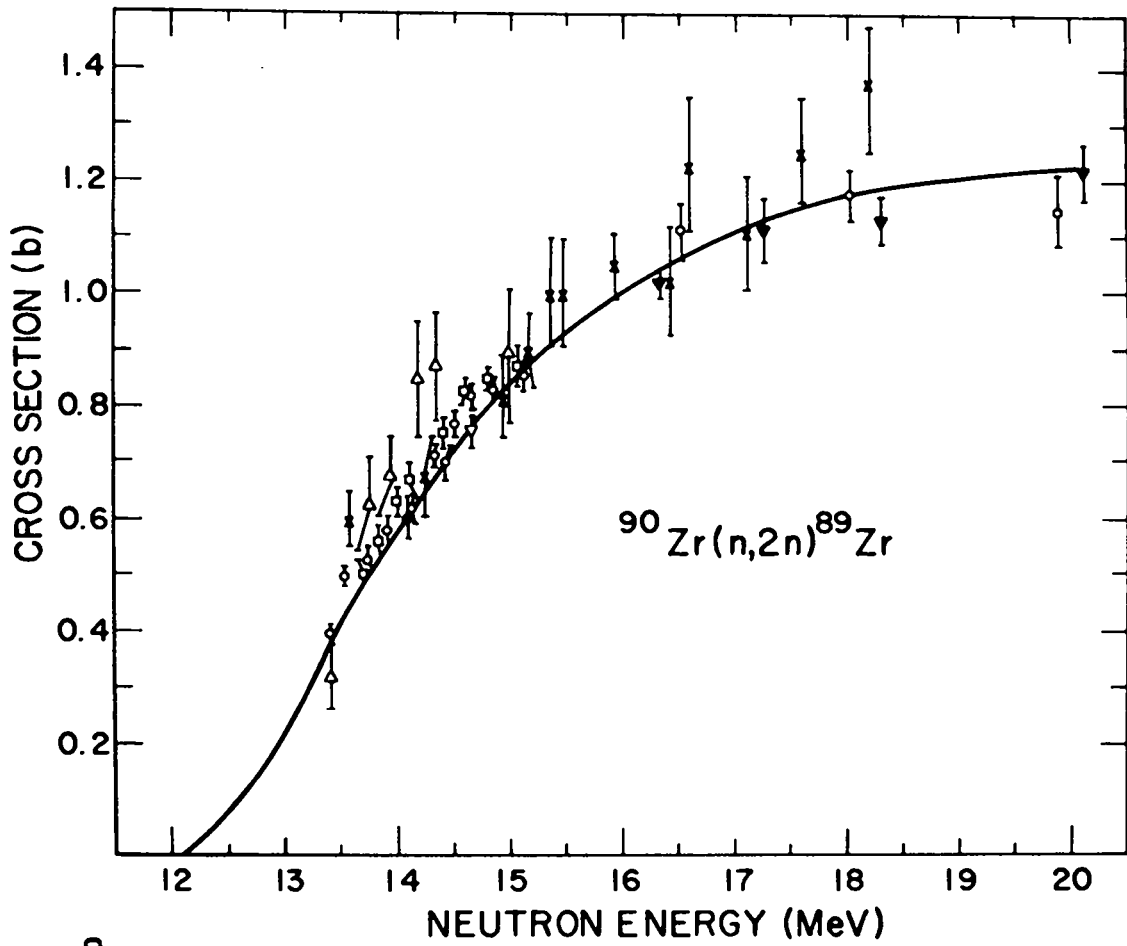
Figure 14. Comparison of calculated cross sections to experimental data for the Zr-90(n,2n) and Sn-112(n,2n) reactions.

TABLE II

TABLE II
SELECTED DATA FOR INDIVIDUAL NUCLIDES

Z	Sym.	A	$\langle R \rangle$[a]	g_0	No. of Levels	G. S.	1st Excited State E	J^π
34	Se	85			1	(5.2+)[b]		
		86	1.19-4[c]		2	0 +	0.704	2 +
		87	6.07-6	8.60[d]	2	(5/2+)	(1.0)	(1/2+)
		88	1.39-5	8.70[d]	2	0 +	(0.76)	(2 +)
		89	2.5 -7		1	(5/2+)		
36	Kr	90			3	0 +	0.7071	2 +
		91	1.41-5		1	5/2+		
		92	1.38-5	8.32	2	0 +	(0.80)	(2 +)
		93	2.3 -5	8.40	2	7/2+	(0.2)	(5/2+)
		94	3.4 -4		1	0 +		
38	Sr	92			10	0 +	0.8147	2 +
		93	3.3 -5		5	(7/2+)	0.21339	(5/2+)
		94	7.74-5	8.04[d]	2	0 +	0.8369	2 +
		95	8.25-6	8.13[d]	6	(7/2+)	0.352	(5/2+)
		96	9.9 -5		2	0 +	0.815	2 +
40	Zr	97			10	1/2+	1.1030	3/2+
		98			7	0 +	0.8530	0 +
		99	4.32-5	7.62	7	1/2+	0.1217	3/2+
		100	1.88-4	7.69	6	0 +	0.2125	2 +
		101	5.63-5		1	(7/2+)		
		102	5.17-4	7.85	5	0 +	0.1519	2 +
		103	5.52-5	7.92	2	7/2+	(0.16)	(1/2+)`
		104	4.74-4		1	0 +		
42	Mo	105			3	(5/2+)	0.095	(7/2+)
		106	1.63-3		4	0 +	0.1717	2 +
		107	2.6 -5	8.23	2	1/2+	(0.13)	(3/2+)
		108	7.4 -5	8.31	2	0 +	(0.12)	(0 +)
		109	2.3 -5		1	1/2+		
50	Sn	128			1	0 +		
		129	2.03-5		11	3/2+	0.035	11/2-
		130	1.02-4	10.00	4	0 +	1.217	2 +
		131	3.8 -6	10.08	5	3/2+	0.334	(1/2+)
		132			2	.0 +	4.041	3 -
54	Xe	135	1.93-5		10	3/2+	0.28845	1/2+
		136	7.91-4		10	0 +	1.3131	2 +
		137	6.29-6	10.54	7	7/2-	0.6010	3/2-
		138	1.99-5	10.62	7	0 +	0.5889	2 +
		139	8.24-6	10.69	2	7/2-	(0.25)	(3/2-)
		140	8.09-5		3	0 +	0.3768	2 +
56	Ba	143			7	(5/2-)	0.0336	(7/2-)
		144	8.25-4		5	0 +	0.1994	2 +
		145	2.97-5	11.15	2	7/2-	(0.1)	(3/2-)
		146	6.00-4	11.23	3	0 +	0.1810	2 +
		147	4.8 -5		1	7/2-		

a. $\langle R \rangle$ is defined in Sec. II.C.
b. Values in parentheses are especially uncertain.
c. 1.19-4 is an abbreviation for 1.19×10^{-4}.
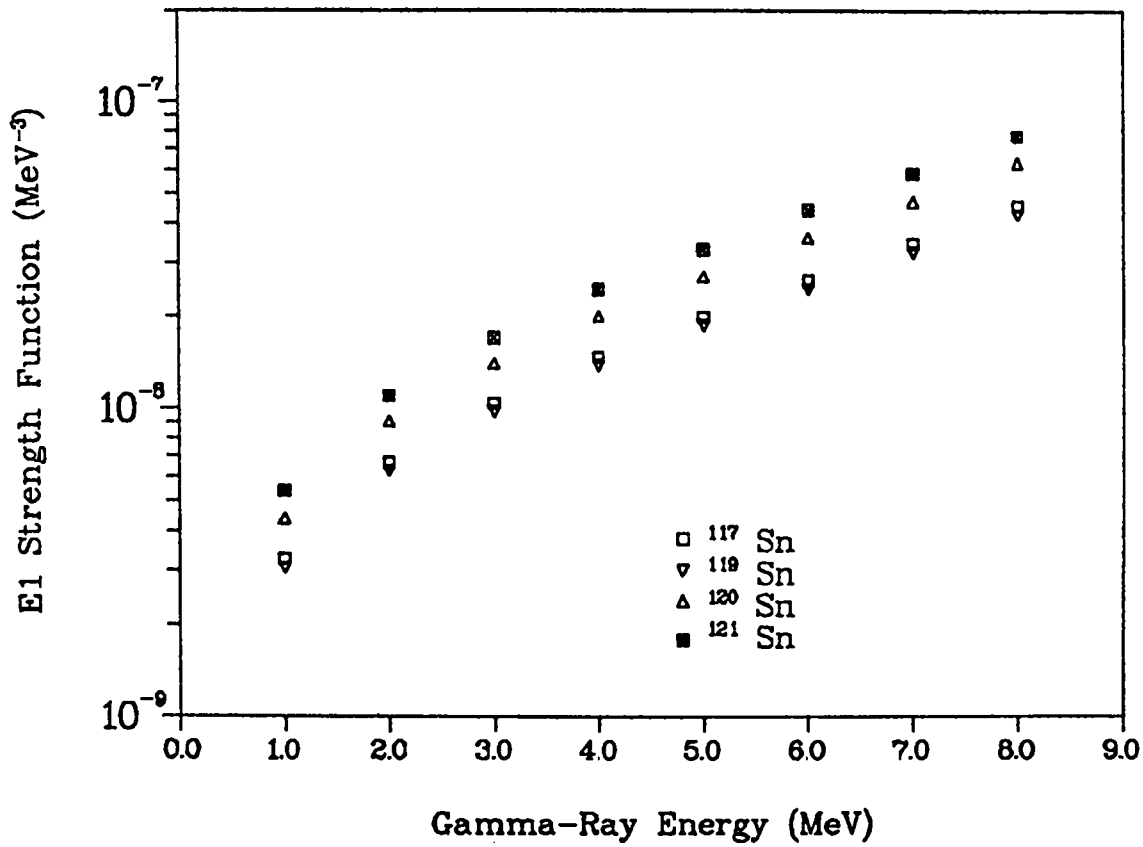d. These values of g_0 are discussed in Sec. II.D.

Figure 15. Gamma-ray strength functions determined from fits to capture data on tin isotopes.

D. Parameters for the Pre-Equilibrium Model

Our treatment of pre-equilibrium processes uses the master equations of Kalbach.[12] In this model, we generally use the value A/13 for the composite-nucleus state-density constant (called g_o in GNASH[5]). Unfortunately, our initial GNASH runs gave unrealistically large pre-equilibrium fractions for relatively low incident-neutron energies for the targets ^{87,88}Se, ^{92,93}Kr, and ^{95}Sr. To correct this, we arbitrarily increased the state density by approximately 30% for all isotopes of these elements, which is sufficient to keep the pre-equilibrium fraction below 0.3 up to incident-neutron energies of 10 MeV. Our values of g_o are included in Table II.

E. Properties of Discrete Levels

Ideally, for each of the 44 nuclides in our data set we should include all of the low-lying discrete states that seem to form a well-understood and reasonably complete block of data (the maximum was 11 levels in ^{129}Sn). We tolerate a few levels with unknown or ambiguous spin or parity if there are better-determined levels above them, and assign plausible parameters to them, relying primarily on shell-model arguments to do so.* Unfortunately, 8 of the 44 nuclides had no experimental information to establish the nature of even the ground state, and there were 14 whose first excited state had unknown spin and parity. Among our 19 target nuclides we found two whose ground-state spin and parity were unknown and nine for which the first excited state has not been observed at all. For the latter we deduced plausible energies from the systematics of nearby nuclides, as well as credible spins and parities, in an attempt to get a more consistent treatment of inelastic scattering. Table II includes the properties assigned to the first and second levels of each of the 44 nuclides.

F. Continuum Level Densities

Above the highest discrete level we have used the Gilbert-Cameron[13] level-density expressions with the Cook[14] parameters. This formulation is based on a systematic study of level spacings near the neutron binding energy, and consists of a constant-temperature approximation at low excitation energies joined smoothly to a Fermi-gas formula at high excitation energies. We suspect that extrapolation of these relations to the extremely neutron-rich region of the fission fragments is the least reliable of our many assumptions.

---

*D. G. Madland gave us invaluable help with these assignments.

G. Ground-State Mass Excesses

Approximately half of the required nuclides lie outside the range for which ground-state mass excesses have been determined experimentally. We have used the adjusted masses from the 1977 Nuclear Wallet Cards. These include many values "estimated from nuclear systematics." Wherever necessary, we have supplemented the tabulated values with extrapolations based on the Garvey-Kelson[15] relations.

III. NOMENCLATURE

In the detailed discussion that follows, we consider a neutron of laboratory energy E_n incident on a target nuclide of mass number A. We describe the initial compound nucleus that results as the "A+1" nuclide. Similarly, we shall label the products of the (n,2n) and (n,3n) reactions the A-1 and A-2 nuclides, respectively.

If the A+1 nuclide emits at least one photon before reaching a stable state, we include that interaction in the "capture" cross section. If the decay of the A+1 compound nucleus ends at the A+1 ground state, we include the interaction in the "activation" cross section. Normally we reserve the designation "(n,γ)" for the activation cross section and the <u>photons</u> emitted by the A+1 nuclide, whereas any <u>neutrons</u> emitted by the A+1 nucleus after the emission of at least one photon are arbitrarily included in the (n,n') cross section and spectrum. For clarity and emphasis, however, we shall occasionally distinguish between an (n,γ) spectrum (consecutive photons emitted from A+1 without neutron emission) and an (n,γ)+(n,γn') spectrum (all photons emitted from A+1). In the ENDF/B output format, we use MT = 102 for the activation cross section and the (n,γ) + (n,γn') photon spectrum. The (n,γn') cross section and its neutron spectrum never appear explicitly in our calculations or output.

IV. COMPUTER PROGRAMS

COMNUC[4] includes in its calculations width-fluctuation corrections that are important at low excitation energies. It calculates angular distributions of neutrons in the Hauser-Feshbach approximation, but does not treat pre-equilibrium processes or calculate continuous spectra of either neutrons or photons. Thus, it is most useful at low incident energies. GNASH[5] calculates neutron and photon spectra but not angular distributions, lacks width-fluctuation corrections, but includes pre-equilibrium effects, so it is most useful at higher E_n, especially above the (n,2n) threshold.

COMNUC is entirely self-contained. Consequently all required input data must be supplied to it on cards. GNASH, on the other hand, takes only the case description from cards, and uses three external files to supply neutron transmission coefficients, level properties, and ground-state mass excesses. We usually use TCCAL* to calculate the transmission-coefficient file, which is used to describe neutron interactions with all nuclides in a given problem. Also, because GNASH treats only the nonelastic part of the interaction with the target nucleus, we calculate the shape-elastic cross section and angular distribution separately, using SCAT.[6]

Since GNASH treats each nuclide independently in a multistep reaction, it yields neutron-emission spectra from each nuclide in turn. It cannot write directly the conventional (n,2n) and (n,3n) spectra, although the corresponding photon spectra are simply those from the A-1 and A-2 nuclides, respectively. In order to permit calculating these higher-multiplicity neutron spectra, GNASH writes detailed bin populations to an external file. A postprocessor named SPECTRA recombines the population information into the (n,n') spectrum and the components of the (n,2n) and (n,3n) spectra that are emitted from each nucleus. Subsequently, we combine these into the final spectra and tabulate the fraction of each spectrum bin that is derived from pre-equilibrium neutron emission from the A+1 nuclide. With this information we can later assign secondary-neutron angular distributions to each bin of each neutron spectrum by applying the systematics developed by Kalbach and Mann.[7]

A.   The GNASH Family

GNASH is best described as the key element in a family of codes and postprocessors, which we shall therefore refer to as the "GNASH family." The relationship of the members of this family to each other and to the other codes involved in our work is diagrammed in Fig. 16, which also summarizes the information flow.

The internal structure of GNASH prevents it from calculating correctly the spectrum of photons from the (n,γn') process simultaneously with the pre-equilibrium process in nuclide A+1. The left-hand box marked GNASH in Fig. 15 represents a "standard" run in which the pre-equilibrium calculation is included and the (n,γn') process is excluded. It sends neutron-population information through SPECTRA for sorting into the components of (n,n'), (n,2n), and (n,3n) spectra.

---

*TCCAL consists primarily of spherical optical-model routines excerpted from COMNUC.
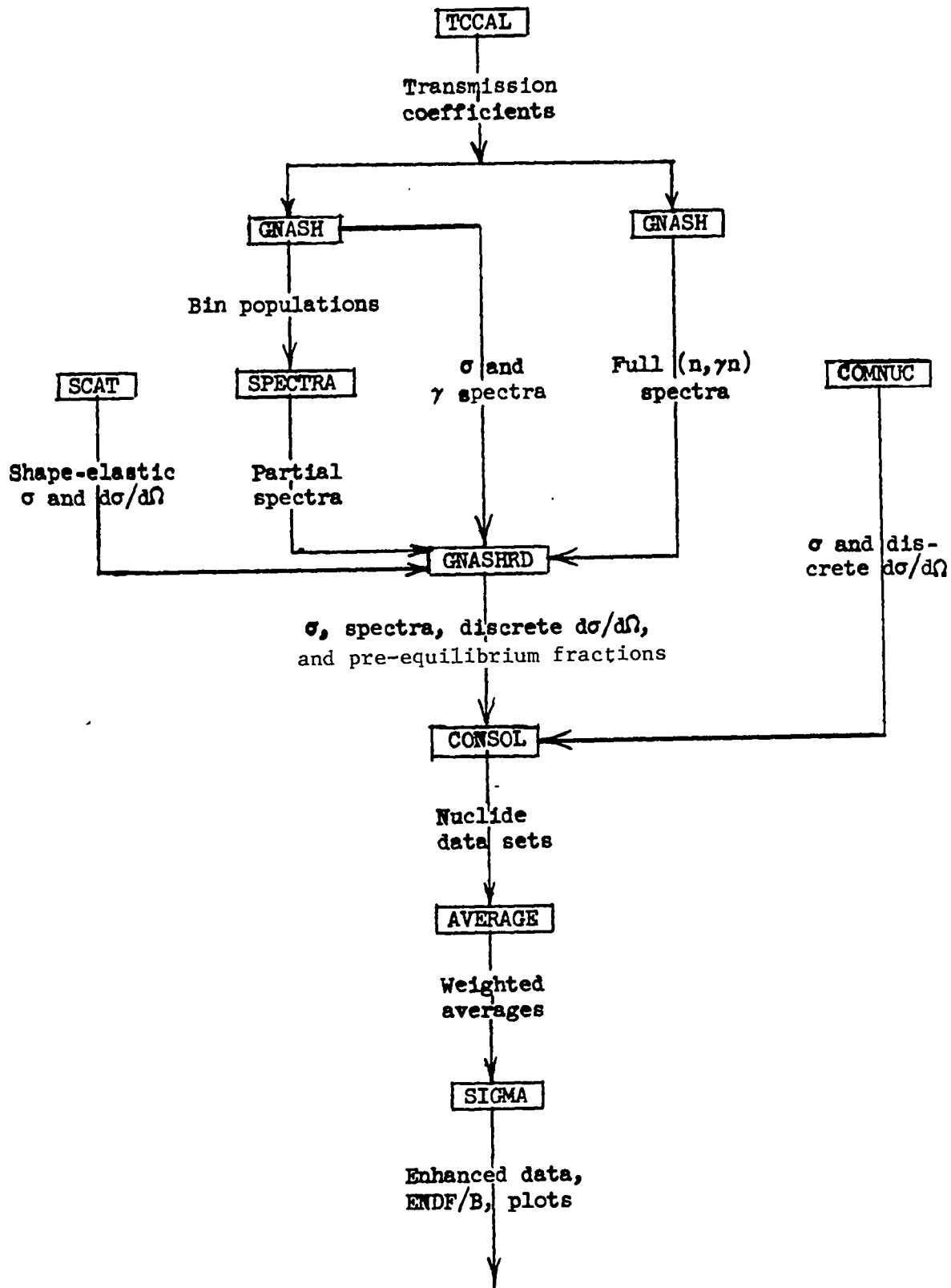
Figure 16. Flow Chart of calculations.

Integrated cross sections and photon spectra go directly to GNASHRD. The right-hand GNASH block represents an independent run in which pre-equilibrium effects are turned off and the full $(n,\gamma)+(n,\gamma n')$ photon spectrum is generated instead.

GNASHRD collects the separate components of the family into a single set of data. It sums the partial neutron spectra to generate $(n,2n)$ and $(n,3n)$ spectra, attaches their composite pre-equilibrium fractions, and adds the shape-elastic cross section from SCAT[6] to the compound-elastic cross section from GNASH. In principle, it also substitutes the full (n,γ) spectrum from the special GNASH run for the incomplete spectrum generated in the standard run.

In practice, we seldom use GNASH to calculate the full (n,γ) spectrum above 5 MeV because it is a very expensive calculation and the cross section becomes very small. Instead, we usually substitute an approximate spectrum above 5 MeV. Discrete levels near the A+1 ground state induce sharp peaks in the low-energy portion of the spectrum. Similarly, the high-energy end of the spectrum acquires pronounced structure from direct transitions from the capturing level to the low-energy discrete levels. The center portion of the spectrum is comparatively smooth.

Accordingly, GNASHRD generates the spectrum above 5 MeV by deforming the 5-MeV spectrum. Keeping the highly structured ends unchanged, it simply "stretches" the smooth center until the discrete transition from the capturing level to the ground state has the correct energy. Then it rebins the distorted spectrum back onto a uniform grid, and normalizes it to a photon multiplicity (extrapolated from the calculated multiplicities at 3 and 5 MeV) that decreases exponentially towards 1.0 at very high E_n. The result is quite similar to the result of actually calculating the spectrum with GNASH.

B.   Combining Results from COMNUC and the GNASH Family

All of our calculations are performed at incident-neutron energies of 0.001, 0.01, 0.03, 0.1, 0.25, 0.5, 1, 2, 3, 4, 5, 6, 8, 10, 12, 14, 16, and 20 MeV. Because of their respective limitations, we restrict the COMNUC calculations to the range 0.001-5 MeV and the GNASH calculations to the range 1-20 MeV. Near 5 MeV the cross sections calculated by the two agree very well, so the main task in generating a complete data set is to effect a smooth transition between 1 and 5 MeV. As indicated in Fig. 16, the composite data set is generated in CONSOL.

CONSOL simply copies the total, elastic, inelastic, and $(n,2n)$ cross sections from COMNUC up to 5 MeV. Above 5 MeV, it copies all neutron cross sections

from GNASHRD. Similarly, it copies photon-production cross sections from GNASHRD above 5 MeV. Between 1 and 5 MeV it multiplies the photon-production cross sections by the COMNUC/GNASH neutron-cross-section ratio and copies the photon spectra from GNASH.

The only cross section that COMNUC does not calculate is the activation cross section. CONSOL copies this from GNASHRD between 1 and 20 MeV. Below 1 MeV, it extrapolates the activation/capture cross-section ratio linearly from the GNASHRD value at 1 MeV to 1.0 at $E_n = 0$, in order to approximate the activation cross section.

COMNUC supplies cross sections and angular distributions for both shape- and compound-elastic scattering up to 5 MeV. GNASHRD supplies the SCAT shape-elastic cross section and angular distribution above 5 MeV. Since the compound-elastic cross section above 5 MeV is less than 3% of the elastic cross section for all of our cases, we ignore its effect on the angular distribution.

The systematic properties of nonelastic secondary-neutron angular distributions analyzed by Kalbach and Mann[7] allow us to assign reasonably reliable angular distributions to each bin of a nonelastic neutron spectrum, since they have found that the distributions are functions only of the secondary-neutron energy and the fraction of the neutrons in that bin that are emitted by the pre-equilibrium process in the A+1 nucleus. Since the present work extends to rather low energies, we have used a modified form of the Kalbach-Mann spectra, which is discussed in the Appendix and illustrated in Fig. 11. We have used these angular distributions for all (n,2n) and (n,3n) spectra, and for (n,n') spectra below the region derived from transitions to discrete levels in the target nucleus. In practice, CONSOL actually generates Kalbach-Mann distributions only for the (n,n') neutrons, and retains the pre-equilibrium fractions for the (n,2n) and (n,3n) spectra so that the angular distributions can be calculated at will later.

Inelastic scattering is the only process for which CONSOL attempts a coordinated treatment of the neutron and photon spectra. Below 5 MeV it produces a discrete inelastic-neutron spectrum that has the appropriately averaged Legendre coefficients (obtained from COMNUC) for the discrete transitions in each bin. It makes no effort to extrapolate these angular distributions above 5 MeV, however, since at higher energies the discrete transitions constitute only a small fraction of the cross section, and they are consequently overwhelmed by the Kalbach-Mann distributions.

Between 1 and 5 MeV, CONSOL uses the wealth of information available from GNASH to reconstruct inelastic photon spectra associated with the COMNUC values for the (n,n') cross section, including contributions from continuum neutrons that feed the photon cascade through discrete levels in the target nucleus. Below 1 MeV it attempts to interpolate both neutron and photon spectra in a consistent manner down to the inelastic threshold.

CONSOL modifies the GNASH $(n,\gamma)+(n,\gamma n)$ spectrum below $E_n = 1$ MeV by the same process that GNASHRD uses above 5 MeV. In compensating for the reduced maximum photon energy, it preserves the structure caused by transitions between discrete levels while uniformly compressing the relatively unstructured middle portion of the spectrum.

C.   Preparation of Finished Data Sets

The output from CONSOL comprises 19 individual data sets (of which ^{138}Xe will be used for both ^{235}U and ^{239}Pu fission fragments). The next program in the sequence (Fig. 15) is AVERAGE, which simply averages 10 data sets together in accordance with the weighting scheme implied by Fig. 1. AVERAGE uses the lowest threshold it finds for each reaction as the threshold for the averaged set.

The last computer program in the chain is SIGMA, which converts each of the data sets from AVERAGE into its final form. Because of constraints imposed by using spectrum bins of finite width, GNASH does not always prepare cross sections and spectra for E_n just barely above the (n,n'), (n,2n), or (n,3n) thresholds. If SIGMA finds a missing neutron cross section in the E_n grid as a result, it interpolates a cross section using an appropriate power-law shape. It also adds several more interpolated points near each of the three thresholds. Then, by interpolating photon multiplicities from 1.0 at threshold to the first calculated multiplicity above threshold, it fills in the corresponding photon-production cross sections near threshold. Finally, it uses spline interpolation to generate intermediate neutron and photon-production cross sections over the entire range of E_n, increasing the E_n grid from 18 to 50 points. The result is shown in Figs. 2 through 5.

COMNUC cannot be used reliably below 1 keV because of probable resonance effects, and it obviously cannot predict detailed slow-neutron cross sections from optical-model parameters. The capture cross section of the ground state of ^{135}Xe dominates the slow-neutron cross section of the fission fragments.

Accordingly, SIGMA uses four straight-line segments on a log-log scale to approximate this cross section below 1 keV, multiplying the isotopic cross section by the known "direct" fast-fission yield of the ^{135}Xe ground state, which is nearly five times as large for ^{239}Pu fission fragments as it is for ^{235}U. The high-energy end of this approximation is simply a log-log extrapolation of the COMUC capture cross section through the point at 1 keV and the splined point at 2 keV. Taking the scattering cross section below 1 keV to be constant, SIGMA then generates the corresponding total cross section, and arbitrarily (and certainly incorrectly) generates a slow-neutron photon-production cross section by assuming that the (n,γ) spectrum and multiplicity are constant below 1 keV. These results are shown in Figs. 6 and 7.

SIGMA rebins all spectra as it reads them in, converting them from the constant-width format used in GNASH to a standard mesh that uses narrower bins at low secondary-neutron energies and progressively wider bins at higher energies. It also generates the Kalbach-Mann angular distributions for the (n,2n) and (n,3n) spectra, using the pre-equilibrium fractions transmitted by CONSOL. Finally, it truncates the last bin in each spectrum to conform to the kinematic limit.

Figures 17 and 18 illustrate the rebinned spectra for neutrons and photons, respectively. The inelastic-neutron spectrum in Fig. 17 is the 12-MeV spectrum shown in Fig. 10 multiplied by the photon-production cross section at that energy.

Since the (n,n') spectrum already has associated angular distributions, derived partly from discrete transitions with explicit angular distributions and partly from Kalbach-Mann systematics, the inelastic angular distribution is rebinned simultaneously with the spectrum, using the same weights as are used for the spectrum. Similarly, the pre-equilibrium fractions for the (n,2n) and (n,3n) spectra are rebinned jointly with the spectra themselves, in order to ensure subsequent generation of the correct angular distributions for each new bin.

D.   Final Output Files

All of the final output arrays generated by SIGMA are stored in binary output files for future use. In addition, they are reduced to ENDF/B (version 5) format for ready distribution to users. Use of ENDF format poses a problem for any data set that relies on the Kalbach-Mann systematics for secondary-neutron spectra because File 6 formats for coupled energy-angle distributions rely on either specified analytical forms or tabular representations of spectra associated with each point on an angular distribution. The Kalbach-Mann representation, on
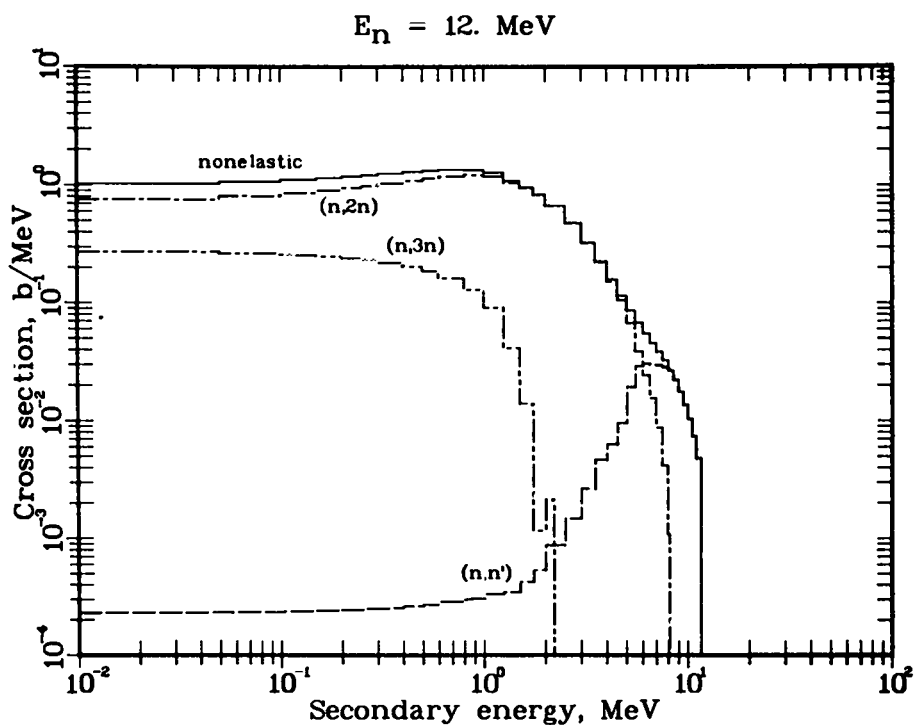
E_n = 12. MeV

Figure 17. Neutron spectra from bombarding ^{235}U fission fragments with 12-MeV neutrons. The (n,n') cross section shown corresponds to the normalized spectrum shown in Fig. 10.
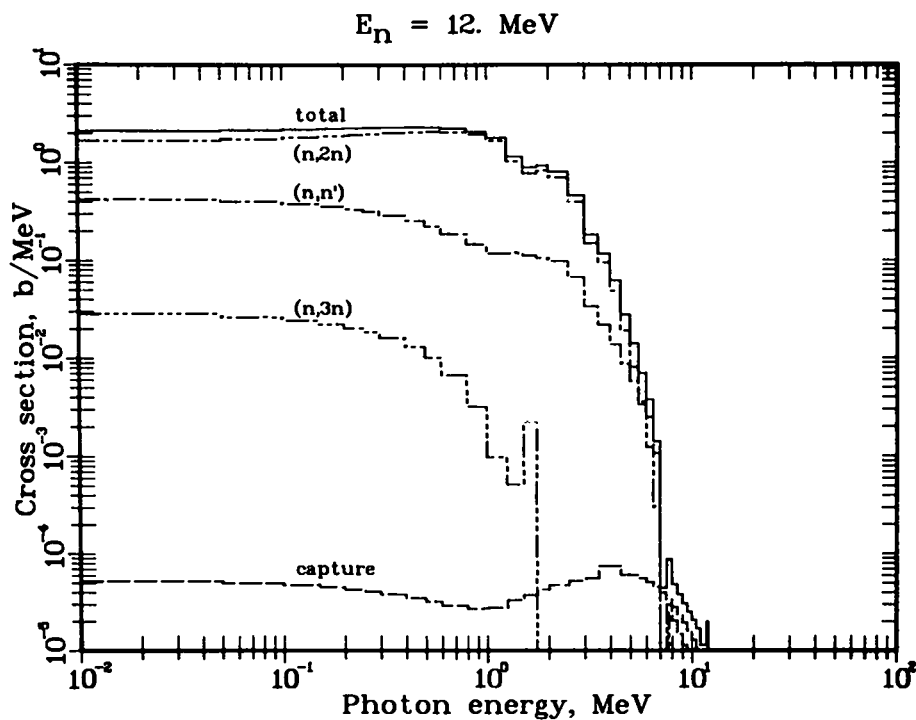
E_n = 12. MeV

Figure 18. Photon spectra from bombarding ^{235}U fission fragments with 12-MeV neutrons.

the other hand, attaches an angular distribution to each bin in a tabulated spectrum. Pending the approval of proposed new formats for File 6, the ENDF/B form of our results currently (August 1981) avoids using File 6, and instead simply has integrated angular distributions in File 4 and integral spectra in File 5.

V. Capture Cross Sections

We have pointed out in Section I that our calculations show that the capture cross section of ^{239}Pu fission fragments is substantially larger than that of ^{235}U fission fragments at almost all energies between 10^{-5} eV and 20 MeV. A complete comparison appears in Fig. 8.* For slow neutrons this is an obvious result of the fivefold greater yield of the ground state of ^{135}Xe from ^{239}Pu fission. Because our weighted averages employ only 10 nuclides each, we have examined the results in more detail to determine whether the factor-of-two difference above 1 keV is caused by the chance behavior of a single nuclide that contributes disproportionately to the average

We note that the neutron separation energy in the A+1 nuclide is systematically slightly larger for the Pu fragments than for the U fragments, which leads directly to the resulting difference in cross sections. At E_n = 1 keV, only two of our sample targets for uranium have capture cross sections greater than 0.1 barn; for plutonium there are four. Furthermore, most of the capture cross section in both averages comes from isotopes of zirconium, but zirconium occurs at the top of the light-fragment peak for ^{239}Pu and at the upper half-height point of the corresponding peak for ^{235}U (see Fig. 1). Thus, the systematic difference in capture cross section can be attributed to the slight displacement of the ^{239}Pu fragments towards higher neutron and proton numbers, relative to the 50-proton closed shell and the closed shells at 50 and 82 neutrons.

REFERENCES

1. E. D. Arthur and D. G. Foster, Jr., "Neutron Cross Section Calculations for Fission-Product Nuclei," Proc. Specialists' Meeting on Neutron Cross Sections of Fission Product Nuclei, Bologna, Italy, December, 1979, Nuclear Energy Agency report NEANDC(E)-209-L, p. 391 (1980).

2. E. D. Arthur and D. G. Foster, Jr., "Average Neutronic Properties of 'Prompt' Fission Products," in "Applied Nuclear Data Research and Development, April 1 – June 30, 1979," Los Alamos Scientific Laboratory report LA-8036-PR, p. 8 (1979).

---

*We thank R. C. Little for supplying this figure.

3. D. G. Foster, Jr., and E. D. Arthur, "Average Neutronic Properties of 'Prompt' Fission Products," in Applied Nuclear Data Research and Development, October 1 - December 31, 1980," Los Alamos National Laboratory report LA-8757-PR, p. 11 (1981).

4. C. L. Dunford, "Compound Nucleus Reaction Analysis Programs COMNUC and CASCADE," Atomics International report TI-707-130-013 (1971).

5. P. G. Young and E. D. Arthur, "GNASH: A Preequilibrium Statistical Nuclear-Model Code for Calculation of Cross Sections and Emission Spectra," Los Alamos Scientific Laboratory report LA-6947 (November 1977).

6. O. Bersillon, "SCAT2 - A Spherical Optical Model Code," in "Progress Report of the Nuclear Physics Division, Bruyeres-le-Chatel, 1977," CEA-N-2037, p. 111 (1978).

7. C. Kalbach and F. M. Mann, "Phenomenology of Continuum Angular Distributions I. Systematics and Parameterization," Phys. Rev. C 23, 112 (1981).

8. E. D. Arthur, "Parameter Determination and Application to Nuclear Model Calculations of Neutron-Induced Reactions on Yttrium and Zirconium Isotopes," Nucl. Sci. Eng. 76, 137 (1980).

9. J. P. Delaroche, Ch. Lagrange, and J. Salvy, "Nuclear Theory in Neutron Nuclear Data Evaluation," IAEA-190, 251 (1976).

10. Ch. Lagrange, "Coherent Optical and Statistical Model Calculations of Neutron Cross Sections for Even A Mo Isotopes," Second Advisory Group Meeting on Fission Product Nuclear Data, Petten, September 1977.

11. C. M. Newstead and J. P. Delaroche, "Evidence for Complex Lane Potential from Strength-Function Measurements," Contrib. Conf. Nuclear Structure Study with Neutrons, Budapest, 1972, J. Erö and J. Szücs, Eds. (Plenum, New York, 1974), p. 142.

12. C. Kalbach, "Exciton-Number Dependence of the Griffin Model Two-Body Matrix Element," Z. Phys. A287, 319 (1978).

13. A. Gilbert and A. G. W. Cameron, "A Composite Nuclear-Level Density Formula with Shell Correctios," Can. J. Phys. 43, 1446 (1965).

14. J. L. Cook, H. Ferguson, and A. R. de L. Musgrove, "Nuclear Level Densities in Intermediate and Heavy Nuclei," Aust. J. Phys. 20, 477 (1967).

15. J. Janecke, "Updated Mass Predictions from the Garvey-Kelson Mass Relations," At. Data Nucl. Data Tables, 17, 456 (1976).

APPENDIX

MODIFIED KALBACH-MANN LEGENDRE COEFFICIENTS

By least-squares fitting to secondary-neutron angular distributions between 20 and 60 MeV, Kalbach and Mann* have derived a simple technique for predicting such distributions with reasonable accuracy. For values of ℓ up to 8, they find that the ENDF/B coefficients can be represented by

$$f_\ell = b_\ell (r_D + r_C \delta) \quad .$$

Here, r_D and r_C are the multistep direct and multistep compound-nucleus fractions ($r_D + r_C = 1$), δ is zero for odd ℓ and unity for even ℓ, and b_ℓ is given by the universal expression

$$b_\ell = \frac{1}{1 + \exp[A_\ell(B_\ell - E)]} \quad , \qquad \text{A-1}$$

in which

$$A_\ell = 0.036 + 0.0039 \; \ell(\ell + 1),$$

$$B_\ell = 92 - 90 \; \sqrt{\ell(\ell + 1)} \quad ,$$

and E is the energy of the secondary neutron. By defining

$$u = A_\ell E$$

and
$$C_\ell = A_\ell B_\ell,$$

we can reduce the expression for b_ℓ to the simple form

$$b_\ell = 1 \Big/ (1 + C_\ell e^{-u}). \qquad \text{A-2}$$

From its form it is clear that b_ℓ is always greater than zero. In particular, $b_1(0) = 0.2241$, which implies substantial forward peaking of the slowest neutrons. The data fitted by Kalbach and Mann, on the other hand, show $b_1(0) \approx 0$, and do not rise as high as the line given by Eq. (A1) until about E =

---

*C. Kalbach and F. M. Mann, "Phenomenology of Continuum Angular Distributions I. Systematics and Parameterization," Phys. Rev. C <u>23</u>, 112 (1981).

30 MeV. Accordingly, we have modified their prescription to eliminate the excessive forward peaking.

Our modification consists of drawing a straight line through the origin that is tangent to b_ℓ, and substituting it for Eq. (A-1) at energies below the point of tangency. The find the point of tangency, we set

$$db_\ell/dE = b_\ell^2 A_\ell C_\ell \exp(-A_\ell E) = b_\ell/E \quad ,$$

and recall that $A_\ell E = u$. We find that the straight line is tangent to the curve at the point where

$$u = 1 + e^u/C_\ell \qquad\qquad\qquad \text{A-3}$$

for any ℓ. Equation (A-3) can be solved very rapidly by iteration, starting with a trial value of $u = 1$, except for $\ell = 1$, for which there is no solution. This results in the constants given in Table A-1, in which the point of tangency is (E_t, b_t).

The "S" shape of the data for b_1 is readily approximated by dividing b_1 in Eq. (A-2) by the factor $1 + \exp[5(0.5-u)]$, which reduces the value of $b_1(0)$ to 0.0170 and is less than 2% smaller than Eq. (A-2) at 30 MeV.

In practice, we truncate the sequence after the last even value of ℓ for which the coefficient is greater than some threshold (e.g., 10^{-3}). The behavior of the modified coefficients up to 100 MeV is shown in Fig. 11.

TABLE A-1
CONSTANTS IN THE MODIFIED KALBACH–MANN RELATIONS

ℓ	A	B	C	E_t	b_t
1	0.0438	28.360	3.4632	–	–
2	0.0594	55.258	2.6637+1[a]	18.671	1.0267−1
3	0.0828	66.019	2.3661+2	12.218	1.1489−2
4	0.1140	71.875	3.6184+3	8.7785	7.5123−4
5	0.1530	75.568	1.0502+5	6.5361	2.5882−5
6	0.1998	78.113	5.9979+6	5.0050	4.5321−7
7	0.2544	79.973	6.8518+8	3.9308	3.9672−9
9	0.3168	81.393	1.5793+11	3.1566	1.7212−11

[a]Abbreviation for 2.6637×10^1.

Page Range	Domestic Price	NTIS Price Code	Page Range	Domestic Price	NTIS Price Code	Page Range	Domestic Price	NTIS Price Code	Page Range	Domestic Price	NTIS Price Code
001-025	$ 5.00	A02	151-175	$11.00	A08	301-325	$17.00	A14	451-475	$23.00	A20
026-050	6.00	A03	176-200	12.00	A09	326-350	18.00	A15	476-500	24.00	A21
051-075	7.00	A04	201-225	13.00	A10	351-375	19.00	A16	501-525	25.00	A22
076-100	8.00	A05	226-250	14.00	A11	376-400	20.00	A17	526-550	26.00	A23
101-125	9.00	A06	251-275	15.00	A12	401-425	21.00	A18	551-575	27.00	A24
126-150	10.00	A07	276-300	16.00	A13	426-450	22.00	A19	576-600	28.00	A25
									601-up	†	A99

†Add $1.00 for each additional 25-page increment or portion thereof from 601 pages up.

Los Alamos